Hopping transport on a randomly substituted lattice for long range and nearest neighbor interactions

Roger F. Loring, Hans C. Andersen, and M. D. Fayer
Department of Chemistry, Stanford University, Stanford, California 94305

(Received 29 July 1983; accepted 28 December 1983)

A theoretical study of hopping transport of excitations or charge carriers among particles randomly distributed on a lattice is presented. The method used is an extension of the diagrammatic technique applied by Gochanour, Andersen, and Fayer to hopping transport in a continuum. We present an exact diagrammatic analysis of the configuration averaged Green function of the Pauli master equation. We obtain a self-consistent approximation to the Green function from which transport properties such as the mean squared displacement may be calculated for any transfer rate, any lattice type and any concentration. For a three dimensional lattice, the results are shown to be accurate in the low concentration limit and for the filled lattice, and are expected to be accurate at intermediate concentration. This is the first theory of hopping transport on a randomly substituted lattice, which is not restricted to low concentration, that can be applied in the case of a long range transfer rate. Results are presented for a Förster dipole–dipole transfer rate and for a transfer rate limited to nearest neighbors for a simple cubic lattice. The latter has a percolation threshold that is described in a qualitatively correct manner by our approximation.

I. INTRODUCTION

The phenomenon of hopping transport in disordered systems is of considerable interest in several areas of solid state physics. The hopping of a carrier between localized states has been demonstrated to be a valid model of electrical transport at high temperature in disordered solids such as amorphous semiconductors[1] and molecularly doped polymers.[2] The radiationless hopping of an electronic excitation among molecular sites has been studied in mixed crystals,[3] solutions,[4] and biological systems,[5] and has recently become a tool for investigating polymer structure.[6]

The radiationless transport of electronic excitations among randomly distributed chromophores has received much theoretical attention. Most workers adopt a model of randomly distributed point chromophores in a continuum.[7] The continuum results of Gochanour, Andersen, and Fayer[8] (hereafter referred to as GAF) show excellent agreement with experiments on dilute dye solutions.[4] Sakun has addressed the problem of energy transport among chromophores distributed randomly on the sites of a lattice, but his results are stated to be valid only at low concentration.[9]

Odagaki and Lax[10(a)] have recently introduced an effective medium approximation for hopping transport on a disordered lattice, but their work is limited to a nearest neighbor transfer rate and to bond disorder rather than site disorder. In the nearest neighbor bond disorder problem, nearest neighbor sites have a given probability of being connected with a bond. The probability that a particular bond exists is uncorrelated with the existence of any other bond. In a site disordered lattice, the system treated here, a lattice site has a given probability of being occupied, and the probability that a site is occupied is uncorrelated with the occupation of any other site. In the site disorder problem with the nearest neighbor transfer rate, a bond exists between adjacent occupied lattice sites. In this case, however, there is a correlation between the existence of a bond connecting a pair of sites and the existence of nearby bonds. Korzeniewski, Friesner, and Silbey[10(b)] have derived an effective medium approximation for transport on a site disordered lattice. They treat transport with a nearest neighbor transfer rate and their method has not been applied to a long range transfer rate.

The electronic excitation transfer rate between two chromophores with a multipolar interaction was shown by Förster[11(a)] and by Dexter[11(b)] to have a $1/r^n$ dependence on the intersite separation. The rate of excitation transfer by an exchange mechanism was shown by Dexter to have an e^{-r} distance dependence.[11(b)] For transfer of charge carriers between majority sites in doped semiconductors, Miller and Abrahams have derived a transfer rate with an $r^{3/2}\,e^{-r}$ distance dependence.[11(c)] Nonnearest neighbor transfer steps can thus be physically important and should not be neglected in a realistic theory. Even in a case in which the tranfer rate falls off very rapidly with distance and the overwhelming majority of hops are between nearest neighbors, transport will be qualitatively different from the predictions of a nearest neighbor hopping model at concentrations below the percolation threshold for the nearest neighbor problem.

In this work we present a theory of hopping transport that can be applied in a straightforward way to calculate transport properties for any transfer rate. We generalize the diagrammatic approach of GAF in the continuum limit to treat transport on a randomly substituted lattice.[12] In Secs. II through IV, we carry out an exact diagrammatic analysis of the ensemble averaged master equation Green function for this problem. In Sec. VI we describe an approximation to the Green function, expected to be valid for any transfer rate, any lattice type, and any concentration. Section VII contains sample calculations for a simple cubic lattice with a nearest neighbor transfer rate and with a Förster dipole–dipole transfer rate. The nearest neighbor results show a site perco-

 0021-9606/84/115731-14$02.10

lation threshold. The results for the Förster rate are shown to be accurate in the high and low concentration limits and are expected to be accurate at intermediate concentration.

II. MASTER EQUATION AND GREEN FUNCTION

We treat a lattice of M sites randomly filled with N particles capable of retaining and transferring an excitation or charge carrier. In the ensuing discussion we adopt the language of energy transfer and refer to these particles as chromophores, but the methods and results apply equally well to the electrical conduction problem. All configurations of the particles are assumed to be equally likely. It follows that a lattice site has a probability $c = N/M$ of being occupied by a chromophore and a probability $1 - c$ of being unoccupied by a chromophore. $p_j(\mathbf{R},t)$, the probability that the jth chromophore is excited at time t in a particular configuration of chromophores $\mathbf{R} = (\mathbf{r}_1,\mathbf{r}_2,\ldots\mathbf{r}_N)$ is taken to satisfy the Pauli master equation:

$$\frac{d\mathbf{p}(\mathbf{R},t)}{dt} = \mathsf{W}\cdot\mathbf{p}(\mathbf{R},t)\,, \tag{II.1}$$

where $p_j(\mathbf{R},t)$ is the jth element of the N-dimensional vector $\mathbf{p}(\mathbf{R},t)$. W is an $N \times N$ matrix given by

$$W_{jk} = w_{jk} - \delta_{jk}\sum_l w_{jl}\,, \tag{II.2}$$

where $w_{jk} = w_{kj}$ is the transfer rate between chromophores j and k, which depends only on the vector distance between the two chromophores. w_{jj} is defined to be zero. δ_{jk} is the Kronecker delta. The decay of $p_j(\mathbf{R},t)$ from lifetime processes has been factored from the problem, as discussed by GAF. The solution to Eq. (II.1) is

$$\mathbf{p}(\mathbf{R},t) = (e^{t\mathsf{W}})\cdot\mathbf{p}(\mathbf{R},0)\,. \tag{II.3}$$

The quantity of interest is the ensemble average excitation probability given by

$$P(\mathbf{r},t) = \left\langle \sum_j \delta_{\mathbf{r}_j,\mathbf{r}}\, p_j(\mathbf{R},t)\right\rangle . \tag{II.4}$$

$P(\mathbf{r},t)$ can be used to define an ensemble average Green function:

$$P(\mathbf{r},t) = \sum_{\mathbf{r}'} G(\mathbf{r},\mathbf{r}',t)\,P(\mathbf{r}',0)\,. \tag{II.5}$$

In the continuum problem treated by GAF, the ensemble average of a configuration dependent function $F(\mathbf{R})$ could be carried out by averaging independently over the position of each chromophore. Here we must average only over configurations in which at most one chromophore occupies any site. The ensemble average of $F(\mathbf{R})$ for the lattice problem is therefore given by

$$\langle F(\mathbf{R})\rangle = \frac{\sum_{\mathbf{r}_1,\ldots\mathbf{r}_N} F(\mathbf{R})\prod_{i<j}(1-\delta_{\mathbf{r}_i,\mathbf{r}_j})}{\sum_{\mathbf{r}_1,\ldots\mathbf{r}_N}\prod_{i<j}(1-\delta_{\mathbf{r}_i,\mathbf{r}_j})}\,. \tag{II.6}$$

The sums over chromophore positions $\mathbf{r}_j$ run over all positions in the lattice. Equations (II.4), (II.5), and (II.6) lead to the following expression for $G(\mathbf{r},\mathbf{r}',t)$:

$$G(\mathbf{r},\mathbf{r}',t) = G^s(\mathbf{r}-\mathbf{r}',t) + G^m(\mathbf{r}-\mathbf{r}',t)\,, \tag{II.7}$$

$$G^s(\mathbf{r}-\mathbf{r}',t) = \delta_{\mathbf{r},\mathbf{r}'}\langle(e^{t\mathsf{W}})_{11}\rangle\,, \tag{II.8}$$

$$G^m(\mathbf{r}-\mathbf{r}',t) = (N-1)\langle\delta_{\mathbf{r}_{12},\mathbf{r}-\mathbf{r}'}(e^{t\mathsf{W}})_{12}\rangle\,. \tag{II.9}$$

$G^s(\mathbf{r}-\mathbf{r}',t) = \delta_{\mathbf{r},\mathbf{r}'}G^s(t)$ gives the probability that a chromophore excited at $t = 0$ retains its excitation at a later time. $G^m(\mathbf{r}-\mathbf{r}',t)$ gives the probability that an excitation located on a chromophore at position $\mathbf{r}'$ at $t = 0$ resides on a chromophore at position $\mathbf{r}$ at a later time. From the Green function, all of the system's transport properties such as the time and distance dependent generalized diffusion coefficient can be calculated. Unfortunately, Eqs. (II.8) and (II.9) cannot be evaluated exactly. The rest of this work will be devoted to the development of an approximation to the Green function, valid at all times and concentrations.

III. PERTURBATION EXPANSION OF THE GREEN FUNCTION

Following GAF, we expand the Fourier–Laplace transform of the Green function in a perturbation expansion. As in their treatment, each term in the expansion will be represented by a diagram. However, because of the difference between the ensemble averaging procedure appropriate to a lattice [see Eq. (II.6)] and that appropriate to a continuum, the diagrams in the lattice problem differ both in structure and in value from those defined by GAF. The Fourier–Laplace transform of $S(\mathbf{r},t)$, a function of lattice vector and time, is defined by

$$\hat{S}(\mathbf{k},\epsilon) = \int_0^\infty dt\, e^{-\epsilon t}\sum_{\mathbf{r}} e^{i\mathbf{k}\cdot\mathbf{r}}S(\mathbf{r},t)\,. \tag{III.1}$$

Applying Eq. (III.1) to Eqs. (II.7) and (II.8) yields

$$\hat{G}^s(\epsilon) = \langle[(\epsilon-\mathsf{W})^{-1}]_{11}\rangle\,, \tag{III.2}$$

$$\hat{G}^m(\mathbf{k},\epsilon) = (N-1)\langle[(\epsilon-\mathsf{W})^{-1}]_{12}e^{i\mathbf{k}\cdot\mathbf{r}_{12}}\rangle\,. \tag{III.3}$$

Equations (III.2) and (III.3) are expanded using the identity

$$(\epsilon-\mathsf{W})^{-1} = \epsilon^{-1} + \epsilon^{-1}\cdot\mathsf{W}\cdot\epsilon^{-1} + \epsilon^{-1}\cdot\mathsf{W}\cdot\epsilon^{-1}\cdot\mathsf{W}\cdot\epsilon^{-1} + \cdots\,. \tag{III.4}$$

We first examine the expansion of Eq. (III.3):

$$\hat{G}^m(\mathbf{k},\epsilon) = (N-1)\sum_{n=1}^{\infty}\epsilon^{-(n+1)}\langle(\mathsf{W}^n)_{12}e^{i\mathbf{k}\cdot\mathbf{r}_{12}}\rangle\,. \tag{III.5}$$

If Eq. (II.2) is substituted into the above, a sum of ensemble averaged products of w_{ij} factors and $-w_{ij}$ factors results. We illustrate our identification of these terms with diagrams in the following example. The contribution to $\hat{G}^m(\mathbf{k},\epsilon)$ that is second order in the transfer rate is

$$\frac{N-1}{\epsilon^3}\left\langle\sum_j W_{1j}W_{j2}e^{i\mathbf{k}\cdot\mathbf{r}_{12}}\right\rangle = \frac{N-1}{\epsilon^3}\left\langle e^{i\mathbf{k}\cdot\mathbf{r}_{12}}\left[\sum_{l\neq 2}(-w_{1l})(w_{12}) + (-w_{12})(w_{12}) + \sum_{m\neq 1}(w_{12})(-w_{2m}) + w_{12}(-w_{21}) + \sum_j w_{1j}w_{j2}\right]\right\rangle . \tag{III.6}$$

The first term on the right-hand side of Eq. (III.6) is rewritten

$$\frac{N-1}{\epsilon^3}\left\langle e^{i\mathbf{k}\cdot\mathbf{r}_{12}}\sum_{l\neq 2}(-w_{1l})\,w_{12}\right\rangle = \frac{(N-1)(N-2)}{\epsilon^3}\langle e^{i\mathbf{k}\cdot\mathbf{r}_{12}}(-w_{13})(w_{12})\rangle\,, \tag{III.7}$$

since each term in the sum over l on the left-hand side of Eq. (III.7) has the same value. Application of Eq. (II.6) yields

$$\begin{aligned}&\frac{1}{\epsilon^3}\frac{(N-1)(N-2)}{(M-1)(M-2)}\sum_{\mathbf{r}_{12},\mathbf{r}_{13}}(-w_{13})(w_{12})\\&\quad\times e^{i\mathbf{k}\cdot\mathbf{r}_{12}}(1-\delta_{\mathbf{r}_1,\mathbf{r}_2})(1-\delta_{\mathbf{r}_1,\mathbf{r}_3})(1-\delta_{\mathbf{r}_2,\mathbf{r}_3})\\&=\frac{1}{\epsilon^3}\frac{(N-1)(N-2)}{(M-1)(M-2)}\sum_{\mathbf{r}_{12},\mathbf{r}_{13}}(-w_{13})(w_{12})\\&\quad\times e^{i\mathbf{k}\cdot\mathbf{r}_{12}}(1-\delta_{\mathbf{r}_2,\mathbf{r}_3})\,.\end{aligned} \tag{III.8}$$

The equality holds because w_{ij} is defined to be zero. In the thermodynamic limit ($N\to\infty, M\to\infty, N/M\to c$), the quantity premultiplying the sum becomes c^2/ϵ^3. Expression (III.8) is represented by a pair of diagrams denoted I and II, shown in Fig. 1, where

$$\begin{aligned}\mathrm{I}&=\frac{c^2}{\epsilon^3}\sum_{\mathbf{r}_{12},\mathbf{r}_{13}}(-w_{13})(w_{12})\,e^{i\mathbf{k}\cdot\mathbf{r}_{12}}\\ \mathrm{II}&=\frac{c^2}{\epsilon^3}\sum_{\mathbf{r}_{12},\mathbf{r}_{13}}(-w_{13})(w_{12})e^{i\mathbf{k}\cdot\mathbf{r}_{12}}(-\delta_{\mathbf{r}_2,\mathbf{r}_3})\,.\end{aligned} \tag{III.9}$$

The ith chromophore is represented by a circle labeled i. A factor w_{ij} is represented by a solid arrow from circle i to circle j. Each solid arrow begins in a solid dot denoted a vertex which carries a value ϵ^{-1}, and ends in a point that may or may not be a vertex depending upon whether it is the beginning of another solid arrow. In the present terminology, an arrow has one beginning and one end, and the arrow head points from the beginning to the end. A factor $-w_{ij}$ is represented by a solid arrow from circle i to circle j followed by a dashed arrow returning to circle i. The last arrow in the diagram, solid or dashed, ends in a vertex. A factor $-\delta_{\mathbf{r}_i,\mathbf{r}_j}$ is represented by a wavy line connecting circles i and j. $\hat{G}^m(\mathbf{k},\epsilon)$ diagrams are characterized by a continuous path of solid and dashed arrows beginning on an initial circle labeled 1 and ending on a final circle labeled 2. Circles 1 and 2 are denoted root circles and other circles visited on the path are denoted field circles. A dashed arrow can only begin at the end of a solid arrow and must return to the circle in which the solid arrow begins.

We define a diagrammatic series γ_m as the sum of all $\hat{G}^m(\mathbf{k},\epsilon)$ diagrams without wavy lines. The diagrams in the series γ_m are the same as those in the series $\hat{G}^m(\mathbf{k},\epsilon)$ in the continuum problem of GAF, which is defined in Eq. (42) of their paper.[8] Of course the value of a γ_m diagram is different from that of the corresponding GAF diagram. Equation (III.5) can now be expressed as a diagrammatic series.

$\hat{G}^m(\mathbf{k},\epsilon)=\gamma_m$ + the infinite series of diagrams constructed by adding to γ_m diagrams at most one wavy line between each pair of circles. Two circles may be connected by a wavy line only if there does not exist a solid arrow that begins in one and ends in the other. (III.10)

A $\hat{G}^m(\mathbf{k},\epsilon)$ diagram in the thermodynamic limit is evaluated as follows. The field circles are assigned dummy labels. Each solid arrow is assigned a factor w_{ij}. Each dashed arrow is assigned a value -1. Each vertex is assigned a factor ϵ^{-1}. Each wavy line is assigned a factor $-\delta_{\mathbf{r}_i,\mathbf{r}_j}$. This product is multiplied by $\exp(i\mathbf{k}\cdot\mathbf{r}_{12})$ and the positions of chromophore 2 and of any field circles are summed over all lattice sites. These sums are unrestricted, since the $\delta_{\mathbf{r}_i,\mathbf{r}_j}$ factors will correct for configurations in which more than one chromophore is allowed to occupy the same site. The result is then multiplied by c^{m-1}, where m is the number of circles in the diagram. Equation (III.10) is an exact result. It is a restatement in diagrammatic language of Eq. (III.3).

Equation (III.2) can be expanded in an analogous fashion to give an exact diagrammatic representation of $\hat{G}^s(\epsilon)$. The diagrams in this series have one root circle labeled 1, one or more field circles, and have a continuous path of solid and dashed arrows that begins and ends on the single root circle. The rules given above concerning allowed sequences of solid arrows, dashed arrows, and vertices in $\hat{G}^m$ diagrams apply here as well. The rules given above for evaluating $\hat{G}^m$ diagrams apply here with the exception of the $\exp(i\mathbf{k}\cdot\mathbf{r}_{12})$ factor included in the evaluation of those diagrams. We define a diagrammatic series γ_s that contains all diagrams with a continuous path of arrows starting and ending on the same circle with no wavy lines. γ_s is the same series as the diagrammatic representation of $\hat{G}^s(\epsilon)$ by GAF in the continuum problem, given in Eq. (28) of their paper. Again, the value of a given γ_s diagram is different from the value of the corresponding GAF diagram. We can then write

$\hat{G}^s(\epsilon)=\epsilon^{-1}+\gamma_s$ + the infinite sum of all diagrams derived from γ_s by introducing wavy lines in the manner described in Eq. (III.10). (III.11)

Like Eq. (III.10), Eq. (III.11) is an exact result. It is a restatement of Eq. (III.2).

IV. RENORMALIZATION OF THE $\hat{G}^m(\mathbf{k},\epsilon)$ SERIES

The diagrammatic expansion of $\hat{G}^m(\mathbf{k},\epsilon)$ [Eq. (III.10)] can be simplified by using a topological reduction procedure, similar to that described by GAF, to eliminate loops. A loop is a part of a diagram that becomes disconnected[13] from both root circles by the removal of a single circle and of a pair of vertices within that circle.[14] The loop does not include this circle. By a procedure analogous to that described by GAF, we can exactly rewrite the diagrammatic series for $\hat{G}^m$ as a new series without loops in which the vertices now carry a

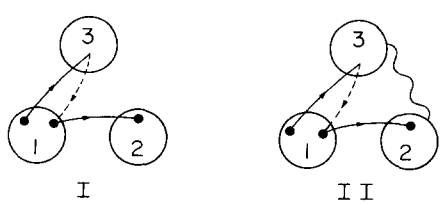

FIG. 1. A pair of diagrams in the expansion of $\hat{G}^m(\mathbf{k},\epsilon)$ given in Eq. (III.10). See Eq. (III.9) and the preceding discussion.

value $\hat{G}^s(\epsilon)$ rather than ϵ^{-1}. Equation (III.10) can be replaced with the following:

$\hat{G}^m(\mathbf{k},\epsilon)$ = the sum of all diagrams in Eq. (III.10) without loops. These diagrams are evaluated by the same procedure as those in Eq. (III.10) except that vertices are assigned the value $\hat{G}^s(\epsilon)$ instead of ϵ^{-1}. (IV.1)

A second topological feature identified by GAF is the node. A node is a vertex in a field circle with the property that removal of the field circle and of that one vertex contained within its leaves the two roots disconnected.[15] The diagrams in $\hat{G}^m(\mathbf{k},\epsilon)$ that have no nodes play a special role. We define $\Sigma[\mathbf{k},\hat{G}^s(\epsilon)]$, the self-energy, by

$$\sum[\mathbf{k},\hat{G}^s(\epsilon)] = \frac{1}{c[\hat{G}^s(\epsilon)]^2}$$

[sum of all diagrams in Eq. (IV.1) without nodes]. (IV.2)

$\Sigma[\mathbf{k},\hat{G}^s(\epsilon)]$ depends on ϵ only through $\hat{G}^s(\epsilon)$. As in the theory of GAF, the sum of all diagrams in $\hat{G}^m(\mathbf{k},\epsilon)$ can be expressed in terms of $\Sigma[\mathbf{k},\hat{G}^s(\epsilon)]$. The result is

$$\hat{G}^m(\mathbf{k},\epsilon) = \frac{c[\hat{G}^s(\epsilon)]^2\,\Sigma[\mathbf{k},\hat{G}^s(\epsilon)]}{1 - c\hat{G}^s(\epsilon)\Sigma[\mathbf{k},\hat{G}^s(\epsilon)]}. \quad \text{(IV.3)}$$

From Eq. (IV.3), we derive an exact relation between $\hat{G}^s(\epsilon)$ and the $k = 0$ limit of $\Sigma[\mathbf{k},\hat{G}^s(\epsilon)]$. The Fourier-Laplace transform of Eq. (II.7) is

$$\hat{G}(\mathbf{k},\epsilon) = \hat{G}^s(\epsilon) + \hat{G}^m(\mathbf{k},\epsilon). \quad \text{(IV.4)}$$

Taking the $k = 0$ limit of Eq. (IV.4) gives

$$\lim_{k\to 0}\hat{G}(\mathbf{k},\epsilon) = \int_0^\infty dt\, e^{-\epsilon t}\sum_{\mathbf{r}} G(\mathbf{r},t) = 1/\epsilon. \quad \text{(IV.5)}$$

Equation (IV.5) is a statement of the conservation of probability. At all times, the excitation must be somewhere in the lattice. Substituting Eqs. (IV.5) and (IV.3) into Eq. (IV.4), and solving for $\hat{G}^s(\epsilon)$, gives

$$\hat{G}^s(\epsilon) = \frac{1}{\epsilon + c\Sigma[0,\hat{G}^s(\epsilon)]}. \quad \text{(IV.6)}$$

Equation (IV.6) resembles the Dyson equation of many body quantum mechanics, with $\hat{G}^s(\epsilon)$ corresponding to a renormalized propagator, ϵ^{-1} corresponding to a bare propagator, and Σ corresponding to a self-energy. If Eqs. (IV.6) and (IV.3) are substituted into Eq. (IV.4), the result is

$$\hat{G}(\mathbf{k},\epsilon) = \left(\epsilon + c\left\{\sum[0,\hat{G}^s(\epsilon)] - \sum[\mathbf{k},\hat{G}^s(\epsilon)]\right\}\right)^{-1}. \quad \text{(IV.7)}$$

Equation (IV.7) has the form of a generalized diffusion equation,[16] with the generalized diffusion coefficient given by

$$\hat{D}(\mathbf{k},\epsilon) = \frac{c}{k^2}\left\{\sum[0,\hat{G}^s(\epsilon)] - \sum[\mathbf{k},\hat{G}^s(\epsilon)]\right\}. \quad \text{(IV.8)}$$

All of the results presented thus far are exact. $\Sigma[\mathbf{k},\hat{G}^s(\epsilon)]$ can, in principle, be calculated by summing the diagrammatic series in Eq. (IV.2). The value of this sum will be a function of the unknown $\hat{G}^s(\epsilon)$. If $\Sigma[\mathbf{k},\hat{G}^s(\epsilon)]$ is evaluated at $k = 0$ and substituted into Eq. (IV.6), the result is an equation with $\hat{G}^s(\epsilon)$ as the only unknown. This equation can then be solved for $\hat{G}^s(\epsilon)$. Substitution of $\hat{G}^s(\epsilon)$ into $\Sigma[\mathbf{k},\hat{G}^s(\epsilon)]$ gives Σ as an explicit function of ϵ. $\Sigma[\mathbf{k},\hat{G}^s(\epsilon)]$ can then be substituted into Eqs. (IV.3) and (IV.7) to calculate the Green function.

V. THE TWO BODY APPROXIMATION TO $\Sigma[\mathbf{k},\hat{G}^s(\epsilon)]$

The diagrammatic series in Eq. (IV.2) cannot in practice be summed exactly to obtain $\Sigma[\mathbf{k},\hat{G}^s(\epsilon)]$. We will follow the procedure of GAF to obtain a self-consistent approximation to $\hat{G}^s(\epsilon)$. First a partial summation of Eq. (IV.2) is carried out that gives an approximation to $\Sigma[\mathbf{k},\hat{G}^s(\epsilon)]$, which depends explicitly on $\hat{G}^s(\epsilon)$. This approximation is substituted into Eq. (IV.6) and the resulting equation is solved for an approximate, self-consistent $\hat{G}^s(\epsilon)$. This approximate $\hat{G}^s(\epsilon)$ can then be substituted into the approximate $\Sigma[\mathbf{k},\hat{G}^s(\epsilon)]$ to give an approximate expression for Σ that depends explicitly on ϵ. This expression for Σ can be substituted into Eq. (IV.7) to calculate an approximation to the Green function. Our approximation scheme is self-consistent[8] in that our approximate $\hat{G}^s(\epsilon)$ and our approximate $\Sigma[\mathbf{k},\hat{G}^s(\epsilon)]$ satisfy Eq. (IV.6). If an arbitrary approximation to $\hat{G}^s(\epsilon)$ is substituted into an arbitrary approximation to the functional $\Sigma[\mathbf{k},\hat{G}^s(\epsilon)]$, evaluation of the right-hand side of Eq. (IV.6), in general, will not give the original approximation to $\hat{G}^s(\epsilon)$. Such an approximation is not self-consistent. In this section we propose a hierarchy of approximations to Σ and evaluate the first member of this hierarchy.

We classify Σ diagrams according to the number of independent particle positions that appear in the summand. A diagram with n circles and no wavy lines has an associated summand that depends on n independent particle positions. The particle positions represented by a set of circles connected by wavy lines are not independent, since a wavy line connecting circles m and n represents a factor $-\delta_{\mathbf{r}_m,\mathbf{r}_n}$. A diagram for which the associated summand depends on i independent particle positions is denoted an i body diagram. $\Sigma[\mathbf{k},\hat{G}^s(\epsilon)]$ can be expressed as

$$\Sigma[\mathbf{k},\hat{G}^s(\epsilon)] = \sum_{i=2}^{\infty}\sum^{(i)}[\mathbf{k},\hat{G}^s(\epsilon)], \quad \text{(V.I)}$$

where $\Sigma^{(i)}$ is the sum of all i body diagrams. We propose a hierarchy of approximations to $\Sigma[\mathbf{k},\hat{G}^s(\epsilon)]$ given by

$$\Sigma[\mathbf{k},\hat{G}^s(\epsilon)] \approx \sum_{i=2}^{n}\sum^{(i)}[\mathbf{k},\hat{G}^s(\epsilon)]. \quad \text{(V.2)}$$

The first member of the hierarchy, the two body approximation, is carried out by setting $n = 2$ in Eq. (V.2). We will sum the $\Sigma^{(2)}$ series exactly as a functional of $\hat{G}^s(\epsilon)$ and use this result with Eq. (IV.6) to obtain an approximate $\hat{G}^s(\epsilon)$.

In their treatment of the continuum transport problem, GAF classify the Σ diagrams according to the number of circles in the diagram. $\Sigma^{(i)}$ in their treatment is defined to be the $i-1$ term in a density expansion of Σ. $\Sigma^{(i)}$ as defined here for the lattice problem contains all of the diagrams in Σ of order c^{i-1}, as well as terms of higher order in c. Our motivation for defining $\Sigma^{(i)}$ as we have, rather than as the $i-1$ term of an expansion of Σ in powers of c, can be illustrated by examining diagram II in Fig. 2. Diagram II was presented as a $\hat{G}^m$ graph in Fig. 1, but since it has neither

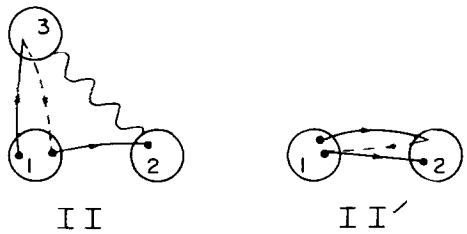

FIG. 2. A pair of diagrams in the expansion of $\Sigma^{(2)}[\mathbf{k},\hat{G}^s(\epsilon)]$, whose values cancel at $c = 1$. See discussion following Eq. (V.2).

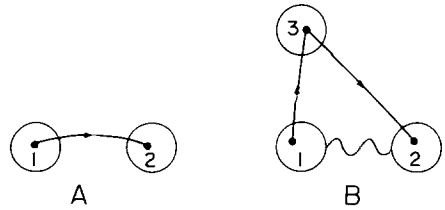

FIG. 3. The two diagrams in the renormalized $\Sigma^{(2)}$ series with nonzero value at $c = 1$. See discussion preceding Eq. (V.3).

loops nor nodes it is also a member of the Σ series. Another diagram can be constructed from II as follows. Move the end of the solid arrow in circle 3 to circle 2. Erase circle 3 and the wavy line connecting circles 2 and 3. The resulting diagram II′, shown in Fig. 2, is a member of the Σ series. If the value of II′ is v, then the value of II is $-cv$. For very small c, diagram II′ makes a more important contribution to Σ than diagram II. For c near 1, the value of II is no longer negligible compared to the value of II′ and at $c = 1$ the value of II exactly cancels the value of II′. If $\Sigma^{(i)}$ were defined simply as the sum of all Σ graphs of order c^{i-1}, the resulting approximation for $\hat{G}^s(\epsilon)$ would be expected to be accurate in the $c \to 0$ limit. Consideration of diagrams such as II and II′ shows that there is no reason to expect such an approximation to be accurate near $c = 1$. $\Sigma^{(2)}$, as we define it here, contains both II and II′. By defining $\Sigma^{(i)}$ in terms of independent particle positions rather than number of circles, we include together with all i circle diagrams, diagrams with more than i circles whose values differ from the values of i circle diagrams by factors of $-c$ and which therefore will not be negligible near $c = 1$. Cancellation at $c = 1$ of the type displayed by diagrams II and II′ is an important feature of the two body approximation and will be discussed further below.

We now carry out the summation of all the diagrams in Eq. (IV.2) with two independent particle positions. In Appendix A, this infinite sum of diagrams is reformulated in a way that is both instructive and useful. We group together sets of diagrams like II and II′ whose values differ only by factors of $-c$ and assign one symbol to their sum. We show in Appendix A that $\Sigma^{(2)}[\mathbf{k},\hat{G}^s(\epsilon)]$ is exactly equal to the subset of diagrams in Eq. (IV.2) with either no field circles or one field circle and a wavy line between the roots. In order to evaluate this set of renormalized diagrams we must define a new topological structure, the moveable part, which is associated with a particular circle. For root circle 1, a moveable part is any end of a solid arrow in the circle. For root circle 2 or a field circle, a moveable part is any end of a solid arrow in the circle except the end of the last solid arrow to visit the circle. The diagrams in this new expansion of $\Sigma^{(2)}$ are evaluated using the same rules that apply to the diagrams in Eq. (IV.2) with one exception. Each circle contributes a factor $Q_n(c)$ to the value of a diagram, where n is the number of moveable parts in the circle. $Q_n(c)$ is an nth degree polynomial in c whose form is given in Eq. (A3) of Appendix A. $Q_0(c) = 1$. For $n > 0$, $Q_n(0) = 1$, and $Q_n(1) = 0$. The $Q_n(c)$ are related to the cumulant polynomials $P_n(c)$ discussed by Yonezawa and Matsubara,[17] Leath and Goodman,[18] and Sakun[9] by $P_{n+1}(c) = cQ_n(c)$.

These renormalized $\Sigma^{(2)}$ diagrams can be divided into two groups. The values of diagrams in the first group contain only $Q_0(c)$ factors and are finite at $c = 1$. Values of diagrams in the second group contain one or more factors of $Q_n(c)$ with $n > 0$ and vanish at $c = 1$. These diagrams represent corrections to $\Sigma^{(2)}$ that account for the correlated hopping characteristic of a disordered system. Although the second group of diagrams contains an infinite number of members, the first group contains just two diagrams, shown in Fig. 3. It is instructive to calculate the generalized diffusion coefficient $\hat{D}(\mathbf{k},\epsilon)$ at $c = 1$ in the two body approximation, from Eq. (IV.8). Since diagram B in Fig. 3 is not $\mathbf{k}$ dependent, it does not contribute to $\Sigma[0,\hat{G}^s(\epsilon)] - \Sigma[\mathbf{k},\hat{G}^s(\epsilon)]$. Therefore, $\hat{D}(\mathbf{k},\epsilon)$ in the two body approximation at $c = 1$ is calculated just from diagram A in Fig. 3. The value of diagram A is $c\Sigma_{\mathbf{r}} \exp(i\mathbf{k}\cdot\mathbf{r})w(\mathbf{r})$. Equation (IV.8) gives

$$\hat{D}(\mathbf{k},\epsilon) = \frac{1}{k^2}\sum_{\mathbf{r}}[1 - \exp(i\mathbf{k}\cdot\mathbf{r})]w(\mathbf{r}) \tag{V.3}$$

at $c = 1$. It can be shown[19] that Eq. (V.3) is exactly the correct result at $c = 1$. Equation (IV.7) shows that if the two body $\hat{D}(\mathbf{k},\epsilon)$ is exactly correct at $c = 1$, then the two body approximation to the full Green function $\hat{G}(\mathbf{k},\epsilon)$ at $c = 1$ must be exactly correct as well. By defining $\Sigma^{(2)}$ as the sum of all Σ graphs with two independent particle positions rather than as the sum of all Σ graphs of order c, we obtain an approximation to $\hat{D}(\mathbf{k},\epsilon)$ that is not only accurate in the limit $c \to 0$ (since it contains all Σ diagrams with at most one factor of c) but that is exact at $c = 1$. We do not prove that recovering the exact $\hat{D}(\mathbf{k},\epsilon)$ at $c = 1$ is a feature of the n body approximation for arbitrary n. The two body results suggest that this may be the case. If it is, then the hierarchy of approximations in Eq. (V.2) represents a well defined way to improve upon the two body approximation.[20]

The reformulation of the $\Sigma^{(2)}$ series carried out in Appendix A is instructive in that the new series is composed of a group of terms with finite values at $c = 1$ and a group of terms with zero value at $c = 1$. It is also useful because the new series is in a form that can conveniently be summed. This summation is carried out in Appendix B. The result is

$$\sum^{(2)}[\mathbf{k},\hat{G}^s(\epsilon)] = \sum_{\mathbf{r}} w(\mathbf{r})\int_0^\infty d\alpha\, e^{-\alpha}\left(\frac{e^{-z\alpha}}{1 - c + ce^{-z\alpha}}\right) \times\left[\frac{1}{c}\ln(1 - c + ce^{-z\alpha}) + \frac{e^{-z\alpha}}{1 - c + ce^{-z\alpha}}(e^{i\mathbf{k}\cdot\mathbf{r}} - 1) + 1\right], \tag{V.4}$$

where $z = w(\mathbf{r})\hat{G}^s(\epsilon)$. The summation runs over all displace-

ments r in the lattice. The integral over α must be done numerically. For a given lattice type and transfer rate, Eq. (V.4) is substituted into Eq. (IV.6) and a numerical solution for $\hat{G}^s(\epsilon)$ can be obtained. This self-consistent $\hat{G}^s(\epsilon)$ can be substituted into Eq. (V.4) and the result substituted into Eq. (IV.8) to obtain an approximation to the generalized diffusion coefficient $\hat{D}(\mathbf{k},\epsilon)$. In the next section we present some numerical calculations based on Eq. (V.4).

VI. RESULTS

In the previous section it was shown that if the two body approximation to $\Sigma[\mathbf{k},\hat{G}^s(\epsilon)]$ is substituted into Eq. (IV.8) for $\hat{D}(\mathbf{k},\epsilon)$, the result is exactly correct at $c=1$. From Eqs. (V.3) and (IV.7), the two body approximation must therefore recover the exactly correct Green function $\hat{G}(\mathbf{k},\epsilon)$ at $c=1$. However, it is true that $\Sigma^{(2)}[\mathbf{k},\hat{G}^s(\epsilon)]$ at $c=1$ is an approximation to $\Sigma[\mathbf{k},\hat{G}^s(\epsilon)]$, which neglects an infinite series of diagrams that have a wavy line connection between the root circles. The values of these diagrams are independent of $\mathbf{k}$, and therefore they would not contribute to $\hat{D}(\mathbf{k},\epsilon)$ in Eq. (IV.8). It can be shown that the two body self-consistent $\hat{G}^s(\epsilon)$, calculated from Eq. (IV.6), is not exactly correct at $c=1$. Since the two body approximation to the full Green function at $c=1$ is exactly correct, the two body approximation to the diagonal part of the Green function must also be exactly correct. The fact that our self-consistent $\hat{G}^s(\epsilon)$ is not exactly correct at $c=1$ implies that the two body $\hat{G}^m(\mathbf{k},\epsilon)$ has a spurious diagonal ($\mathbf{k}$ independent) contribution that cancels the error in $\hat{G}^s(\epsilon)$ so that the sum $\hat{G}(\mathbf{k},\epsilon)=\hat{G}^s(\epsilon)+\hat{G}^m(\mathbf{k},\epsilon)$ is correct at $c=1$. The exactly correct $\hat{G}^m(\mathbf{k},\epsilon)$ has no diagonal contribution.

We can test the accuracy of our two body $G^s(t)$ calculation at $c=1$ by examining the case of nearest neighbor hopping on a filled simple cubic lattice. $G^s(t)$ cannot be calculated exactly in closed form for a filled lattice of arbitrary type and a transfer rate of arbitrary distance dependence. However, for the case of a transfer rate that is nonzero only between nearest neighbors on a filled simple cubic lattice, $G^s(t)$ may be calculated exactly[21]:

$$G^s(t)=[e^{-2wt}I_0(2wt)]^3\,, \tag{VI.1}$$

where w is the magnitude of the step rate and I_0 is a modified Bessel function. Figure 4 shows plots of the exact $G^s(t)$ (A) and the two body approximate $G^s(t)$ (B) for this case. The approximate curve was calculated by substituting Eq. (V.4) into Eq. (IV.6), evaluating $\hat{G}^s(\epsilon)$ numerically and then inverting the Laplace transform numerically using the Stehfest algorithm.[22] Figure 4 shows that the approximate $G^s(t)$ is practically indistinguishable from the exact answer in this case. The error in $\hat{G}^s(\epsilon)$ at $c=1$ and hence the spurious diagonal contribution to $\hat{G}^m(\mathbf{k},\epsilon)$ must be small for the case of a nearest neighbor transfer rate on a cubic lattice. We have also compared the two body $G^s(t)$ for nearest neighbor hopping on a filled square lattice with the exact result. The agreement is less good than the agreement between the approximate and exact $G^s(t)$ for a cubic lattice, indicating that the two body results may be less accurate in two dimensions than in three.

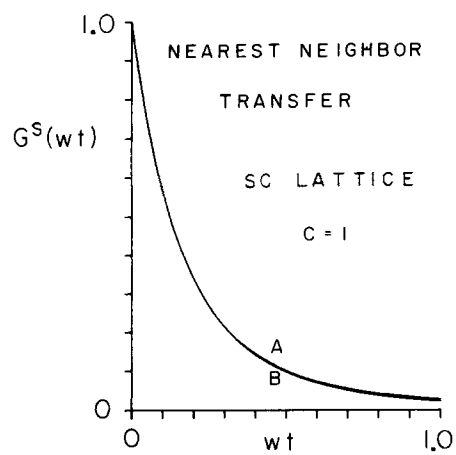

FIG. 4. $G^s(t)$, the probability that an initially excited chromophore retains its excitation after a time t for a simple cubic lattice and a nearest neighbor transfer rate. Curve A is the exact result [Eq. (VI.1)], and curve B is the two body result. The two body approximation is highly accurate for this case.

Another transport property that can be calculated in a straightforward way from our formalism in the two body approximation is the time dependent mean squared displacement of an excitation. The Laplace transform of the mean squared displacement along the $\hat{k}$ direction is given by

$$\langle[\mathbf{r}(\epsilon)\cdot\hat{k}\,]^2\rangle=(2/\epsilon^2)\lim_{|\mathbf{k}|\to 0}\hat{D}(\mathbf{k},\epsilon)\,, \tag{VI.2}$$

provided that the symmetry of the problem is such that $\langle\mathbf{r}(\epsilon)\cdot\hat{k}\,\rangle=0$. The overall mean squared displacement on a d-dimensional lattice is given by

$$\langle r^2(\epsilon)\rangle=(2/\epsilon^2)\sum_{i=1}^{d}\hat{D}_{x_i}(\epsilon)\,. \tag{VI.3}$$

$\{\hat{x}_i\}$ is a set of d mutually orthogonal unit vectors and $\hat{D}_{x_i}(\epsilon)$ is the limit as $|\mathbf{k}|$ approaches 0 of $\hat{D}(\mathbf{k},\epsilon)$, where $\mathbf{k}$ is taken to point in the $\hat{x}_i$ direction. In many situations of interest, the limit as $|\mathbf{k}|\to 0$ of $\hat{D}(\mathbf{k},\epsilon)$ does not depend on $\hat{k}$. For these situations we have

$$\langle r^2(\epsilon)\rangle=(2d/\epsilon^2)\hat{D}(0,\epsilon)\,. \tag{VI.4}$$

If the limit $\epsilon\to 0$ of $\hat{D}_{x_i}(\epsilon)$ exists for all i, then $\langle r^2(\epsilon)\rangle$ will grow linearly with time in the long time limit with slope

$$2\sum_{i=1}^{d}\hat{D}_{x_i}(0)\,.$$

For the situation described by Eq. (VI.4), $\langle r^2(\epsilon)\rangle$ will have slope $2d\hat{D}(0,0)$ in the long time limit.

From Eqs. (IV.8), (V.4), and (VI.2), we can calculate a general expression for $\langle r^2(\epsilon)\rangle$ in the two body approximation

$$\langle r^2(\epsilon)\rangle=c/\epsilon^2\sum_{\mathbf{r}}r^2w(\mathbf{r})\int_0^\infty d\alpha\left[\frac{e^{-z\alpha}}{1-c+ce^{-z\alpha}}\right]^2 e^{-\alpha}\,,$$
$$z=w(\mathbf{r})\hat{G}^s(\epsilon)\,. \tag{VI.5}$$

If c is set to unity in Eq. (VI.5) we obtain the exact result for a filled lattice:

$$\langle r^2(\epsilon)\rangle=1/\epsilon^2\sum_{\mathbf{r}}r^2w(\mathbf{r})\,. \tag{VI.6}$$

In Fig. 5 we show the time derivative of the mean squared

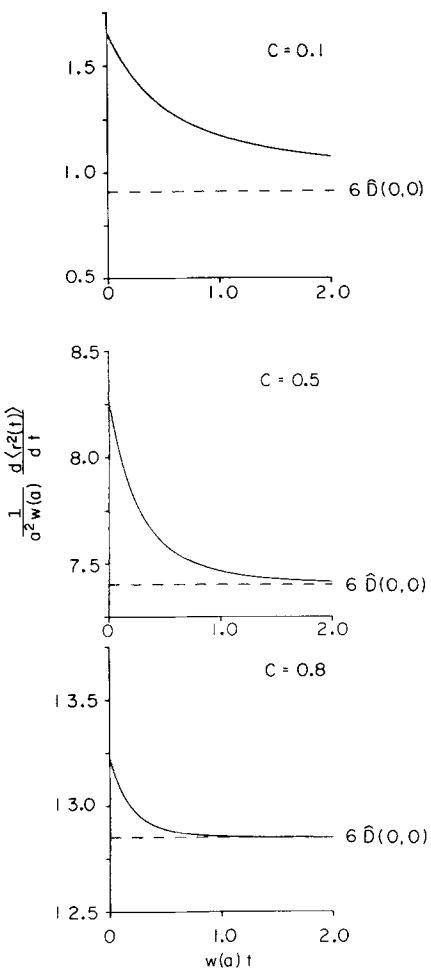

FIG. 5. The concentration dependence of the diffusion constant $\hat{D}(0,0)$ in the two body approximation for a nearest neighbor transfer rate (N) and for a Förster dipole–dipole transfer rate (F) on a simple cubic lattice of spacing a. $w(a)$ is the nearest neighbor step rate. The dashed curve shows $\hat{D}(0,0)$ for the Förster rate in a continuum with a chromophore number density c/a^3 in the two body approximation of GAF.

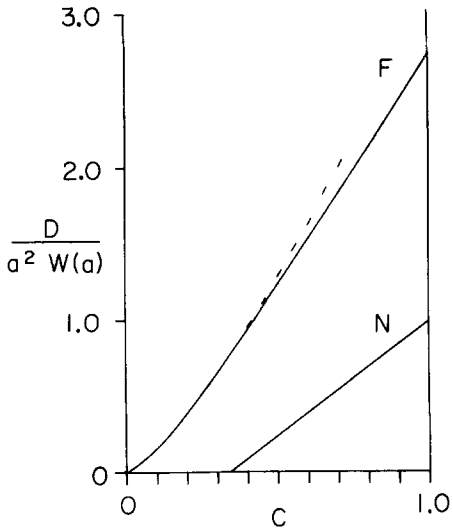

FIG. 6. The time dependence of the time derivative of $\langle r^2(t)\rangle$, the mean squared displacement, in the two body approximation for a Förster transfer rate on a simple cubic lattice is shown at three concentrations. The dashed line in each plot is $6\hat{D}(0,0)$, the long time limit of this derivative. Transport approaches the diffusive limit more rapidly for higher concentration.

displacement as a function of time for the orientationally averaged Förster dipole–dipole tranfer rate $w(r) = 1/\tau(R_0/r)^6$ on a simple cubic lattice. These plots were calculated in the two body approximation from Eqs. (V.4), (IV.6), and (VI.5). We find for this lattice and transfer rate that within the two body approximation, the limit as t approaches ∞ of $\langle r^2(t)\rangle$ is $6\hat{D}(0,0)t$. $\hat{D}(0,0)$ is a function of c. Figure 5 illustrates that transport becomes diffusive at shorter time for higher concentration. The short time behavior shown in Fig. 5 is quite different from the short time behavior for a continuum discussed in Refs. 7(a) and 8. These authors show that the mean squared displacement for a Förster transfer rate in a continuum goes as $t^{5/6}$ as $t\to 0$. Hence, its derivative diverges as $t\to 0$. It can be demonstrated that the $t\to 0$ limit of $\langle r^2(t)\rangle$ for the lattice two body approximation is $\langle r^2(t)\rangle = c[\Sigma_{\mathbf{r}} r^2 w(\mathbf{r})]t$ and that this is also exactly the correct result.[23] Therefore the $t\to 0$ limit of $d\langle r^2(t)\rangle/dt$ for a lattice exists and equals $c\Sigma_{\mathbf{r}} r^2 w(\mathbf{r})$.

Curve F in Fig. 6 shows the concentration dependence of $\hat{D}(0,0)$ on a simple cubic lattice of spacing a for the orientationally averaged Förster transfer rate. At $c = 1$, the two body $\hat{D}(0,0)$ takes on the exact value for an ordered lattice calculated by Förster.[11(a)] In the limit of low concentration, $\hat{D}(0,0)$ approaches $3.26\,(R_0^6/\tau)\rho^{4/3}$, where $\rho = c/a^3$ is the chromophore number density. This $\rho^{4/3}$ dependence is to be expected since in the limit of low concentration and long time, the lattice will cease to be important and transport should resemble that in a continuum, whose $\hat{D}(0,0)$ must scale[7(a)] as $\rho^{4/3}$. The numerical coefficient is identical to that of the two body GAF $\hat{D}(0,0)$, which is believed to be a good approximation for a continuum. The only effect of the three body corrections calculated by GAF on $\hat{D}(0,0)$ is to lower the multiplicative constant by 11%. The three body results of GAF are in excellent agreement with experiments on dilute dye solutions.[4] Thus the two body lattice $\hat{D}(0,0)$ shown in curve F of Fig. 6 has the exactly correct value at $c = 1$, approaches an accurate continuum approximation at low concentration and hence is expected to be accurate at intermediate concentration.

We next consider the concentration dependence of $\hat{D}(0,0)$ for a nearest neighbor transfer rate. This problem has a percolation threshold. Below the critical concentration for site percolation, the chromophores exist only in clusters of finite size. The mean squared displacement cannot grow linearly with time and $\hat{D}(0,0)$ should be zero. Above the critical concentration, transport on the infinite cluster should become diffusive at long time and $\hat{D}(0,0)$ should be finite. Curve N in Fig. 6 shows the concentration dependence of $\hat{D}(0,0)$ in the two body approximation for a nearest neighbor transfer rate of magnitude w on a simple cubic lattice of spacing a. $\hat{D}(0,0)$ has the exactly correct value at $c = 1$, approaches zero as c approaches 0.353 from above, and is zero below this concentration. The critical concentration for site percolation on a simple cubic lattice has been calculated by Monte Carlo techniques to be 0.312.[24(a)] Thus the two body $\hat{D}(0,0)$ has a physically reasonable concentration dependence. We have also calculated the critical concentration for body centered and face centered cubic lattices. The results are 0.256 and 0.168, respectively. The site percolation thresholds on

these lattices have been estimated by a series expansion technique to be 0.245 ± 0.004 and 0.198 ± 0.003, respectively.[24(b)]

It can be shown that the $\hat{D}(0,0)$ shown in curve N in Fig. 6 vanishes as $(c - c_0)$ as $c \to c_0 +$, where c_0 is the critical concentration. Moreover, the concentration dependence of $\hat{D}(0,0)$ is very close to, though not exactly, linear for all $c > c_0$. This behavior is very similar to the concentration dependence of the diffusion constant in the nearest neighbor transfer problem predicted by the effective medium approximations (EMA) of Odagaki and Lax[10(a)] and Korzeniewski, Friesner, and Silbey.[10(b)] The effective medium approximation predicts an exactly linear concentration dependence of the diffusion constant and a critical concentration $c_0 = 2/z$, where z is the number of nearest neighbors.[25] Our predicted values of c_0 for the cubic lattices are close to but not exactly equal to $2/z$. In fact, it can be shown that the c_0 predicted from our approximation approaches $2/z$ in the $z \to \infty$ limit. The two body approximation presented here has several important differences from the EMA of Refs. 10(a) and 10(b). In order to carry out an EMA calculation for a partially filled lattice, one must first solve exactly the corresponding filled lattice problem. This is not a feature of our approximation. The EMA results of Refs. 10(a) and 10(b) are not readily applicable to a transfer rate of arbitrary distance dependence, whereas the results presented here may be used in a straightforward way to calculate transport properties for any transfer rate.

For the nearest neighbor transfer problem, it can be shown that the $t \to \infty$ limit of the exact $G^s(t)$ is zero at $c = 1$, and is finite at all concentrations below $c = 1$:

$$\lim_{t \to \infty} G^s(t) = [\langle N_c \rangle / N] , \tag{VI.7}$$

where N is the number of chromophores and N_c is the number of clusters in a given configuration. The brackets denote a configuration average. The right-hand side of Eq. (VI.7) is finite for all $c < 1$ and approaches unity as c approaches zero.[22] Our two body $G^s(t)$ for this problem decays to zero as $t \to \infty$ for $c > 0.353$, which casts some doubt on the validity of the two body approximation for a transport problem with critical behavior. Below $c = 0.353$, the two body $G^s(t)$ behaves in qualitatively correct fashion, decaying to a finite value as $t \to \infty$. This limiting value approaches unity as c approaches zero.

VII. SUMMARY

We have presented an exact diagrammatic analysis (Secs. III and IV) of the ensemble averaged Green function for hopping transport of excitations or charge carriers among particles distributed randomly on a lattice. We have proposed a hierarchy of self-consistent approximations to the Green function from which transport properties such as $G^s(t)$, the probability that a particle excited at $t = 0$ retains the excitation at time t, and $\langle r^2(t) \rangle$, the mean squared displacement, can be calculated. The procedure presented here can be applied to any lattice type in which the sites are related by symmetry operations (including lattices with more than one site per unit cell), and any transfer rate. The first member of the hierarchy, the two body approximation, is demonstrated to be accurate for a three-dimensional lattice at unit concentration and in the low concentration continuum limit. This is the first theory of incoherent transport on a randomly filled lattice that can be readily applied to the physically important case of a long range transfer rate.

ACKNOWLEDGMENTS

The authors thank M. D. Ediger and G. H. Fredrickson for useful discussions. R. F. L. thanks the National Science Foundation for a Predoctoral Fellowship. This work was supported by the National Science Foundation through grants CHE81-07165 (HCA) and DMR79-20380 (MDF and RFL). MDF acknowledges the Simon Guggenheim Memorial Foundation for Fellowship support that contributed to this research.

APPENDIX A: RENORMALIZATION OF THE $\Sigma^{(2)}[\mathbf{k}, \hat{G}^s(\epsilon)]$ SERIES

In this Appendix, we derive the renormalized expansion of $\Sigma^{(2)}[\mathbf{k}, \hat{G}^s(\epsilon)]$ presented in Sec. V. The simplification of the $\Sigma^{(2)}$ series presented in Sec. V is based on two different types of cancellation among the diagrams. We first simplify the series by removing a subset of the diagrams whose values sum to zero for all values of c. We then group together sets of diagrams whose values sum to zero at $c = 1$.

In examining a $\Sigma^{(2)}$ diagram, it is useful to group the circles into sets such that all circles in a given set are connected to each other by wavy lines and circles in one set are not connected to circles in another set by wavy lines. Each $\Sigma^{(2)}$ diagram contains two such sets of circles. If a circle has no wavy line connections, it is considered to be a set. We group together diagrams that are topologically similar. Two diagrams are topologically similar if they differ only in the placement of wavy lines among circles in a set. Figure 7 shows two groups of topologically similar diagrams. Diagrams I–IV are topologically similar as are diagrams V–VIII. The values of two topologically similar diagrams are either identical or differ by a factor of -1. When the values of a group of topologically similar diagrams are summed, there will be considerable cancellation. We make use of this cancellation to simplify the $\Sigma^{(2)}$ series by rewriting it as a new series with restrictions on allowable wavy line connections.

A set of circles in a $\Sigma^{(2)}$ diagram either contains no root, one root, or both roots. In diagrams I–IV in Fig. 7, each set contains one root, and in diagrams V–VIII, one set contains both roots and one set contains a field circle. For reasons that will be discussed below we treat a set containing zero or one root differently from a set containing both roots. Consider diagrams I–IV. If the value of I is u, then the value of the sum of I through IV is $2u$. This result could have been predicted from the topological theorem given in Appendix C. If we designate circle 2 as the trunk circle and circles 3 and 4 as branch circles and recall that the circles are distinguishable by the order in which they are visited by solid arrows, then the theorem tells us that we need only retain the diagram in which the circles are linked by a singly connected path of wavy lines that is constructed by drawing a wavy line from

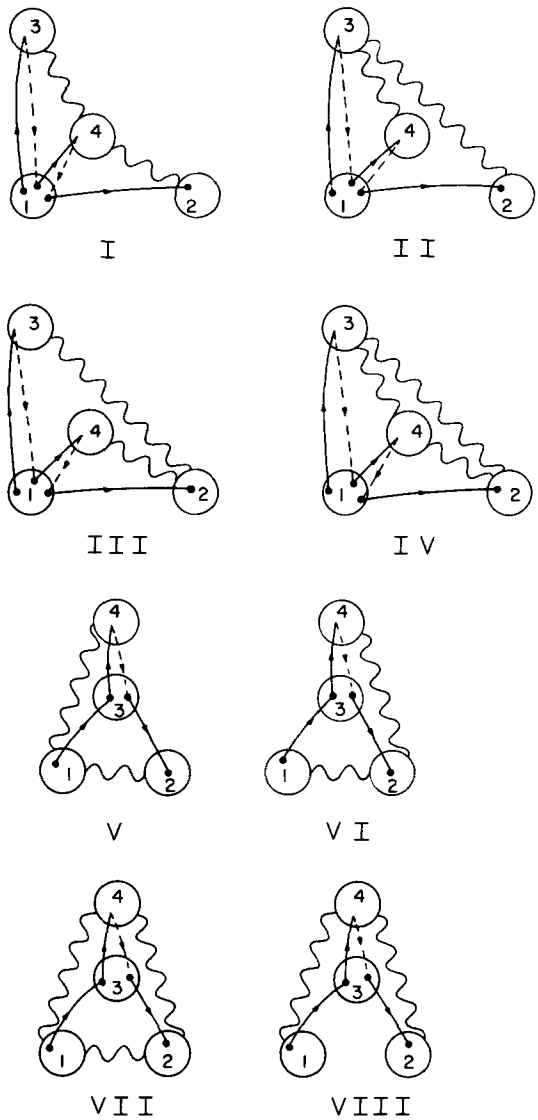

FIG. 7. Two groups of topologically similar $\Sigma^{(2)}$ diagrams. Diagrams I–IV are topologically equivalent, as are diagrams V–VIII.

each circle in the set to the next circle to be visited by solid arrows. The value of this diagram will have an additional factor of $(n-1)!$, where n is the number of circles in the set. Applying the theorem to the sum of I through IV, we see that the sum can be represented by diagram I with an extra factor of $(3-1)!$ and hence that the value of the sum is $2u$. We can thus simplify the $\Sigma^{(2)}$ series by only retaining diagrams in which sets of circles containing zero or one root are connected by a singly connected path of the type just described. Each such set of n circles contributes a factor of $(n-1)!$ to the value of the diagram. This procedure is valid because the topological theorem of Appendix C can be applied independently to each of the two sets of circles in a $\Sigma^{(2)}$ diagram.

We now turn to sets of circles containing both roots as in diagrams V through VIII. For this case we designate the roots as trunk circles and field circle 4 as a branch circle. The topological theorem tells us that we need only retain diagrams in which a wavy line connects the roots and circle 4 is attached by a wavy line either to root 1 or to root 2, but not to both. This connection carries a value 1!. Thus the theorem predicts that the value of the sum of diagrams V–VIII equals the value of the sum of diagrams V and VI. This can be verified by noting that the values of diagrams VII and VIII sum to zero. In general, the theorem in Appendix C tells us that we need only retain diagrams with the following sort of wavy line connections among circles in a set that contains both roots. The roots are connected by a wavy line. The other circles are grouped into two subsets, one of which may be empty. Each subset is linked by a singly connected path of wavy lines constructed by drawing a wavy line from each circle to the next circle in the subset to be visited by solid arrows. The first circle in one subset is connected by a wavy line to one of the roots and the first circle in the other subset is connected to the other root. If one subset has m_1 circles and the other has m_2 circles, then the value of the diagram contains a factor $m_1!m_2!$.

We have simplified the diagrammatic expansion of $\Sigma^{(2)}$ by grouping together diagrams whose values differ only by factors of -1 for all concentrations. We now group together diagrams whose values differ only by factors of $-c$. A necessary concept is that of the reduced diagram. Consider a $\Sigma^{(2)}$ diagram with wavy lines. The corresponding reduced diagram is constructed by collapsing all wavy lines except for a wavy line that connects the roots. Consider two circles A and B linked by a wavy line, where A is visited by solid arrows before B. The wavy line is collapsed by moving all ends of solid arrows in circle A to circle B and then removing circle A and the wavy line. Diagrams without wavy lines and diagrams in which the only wavy line connection is between the roots are their own reduced diagrams. The reduced diagram constructed in this way is always itself a member of the $\Sigma^{(2)}$ diagrammatic series. If a wavy line connecting the roots is collapsed, the result is not a member of the $\Sigma^{(2)}$ series. It is for this reason that we treated sets of circles containing both roots differently from sets of circles containing zero or one root. If a set of circles in a diagram contains zero or one root, then collapsing all wavy lines in that set yields another member of the $\Sigma^{(2)}$ series. In Fig. 8, diagrams I–V have V as a reduced diagram and diagrams VI and VII have VII as a reduced diagram.

Two diagrams that have the same reduced diagram have values that differ only by factors of $-c$. The $\Sigma^{(2)}$ series is renormalized by grouping together all diagrams corresponding to a given reduced diagram and by representing this group with the reduced diagram, which now has a value equal to the sum of the values of the diagrams in the group. The value of this diagram in the renormalized $\Sigma^{(2)}$ series equals the value of the diagram in the original $\Sigma^{(2)}$ series multiplied by a polynomial in $-c$. For example, if the value of diagram V in Fig. 8 is u, then the value of the sum of diagrams I–V is $u(1-3c+2c^2)$. Diagrams I–V in the old $\Sigma^{(2)}$ series are represented in the new $\Sigma^{(2)}$ series by diagram V, where the value of diagram V now includes a factor $1-3c+2c^2$. Similarly diagrams VI and VII in the original series are represented by diagram VII in the renormalized series, where the value of diagram VII now includes a factor of $1-c$.

Each circle in a renormalized Σ diagram has an associated polynomial. This is a reflection of the fact that the

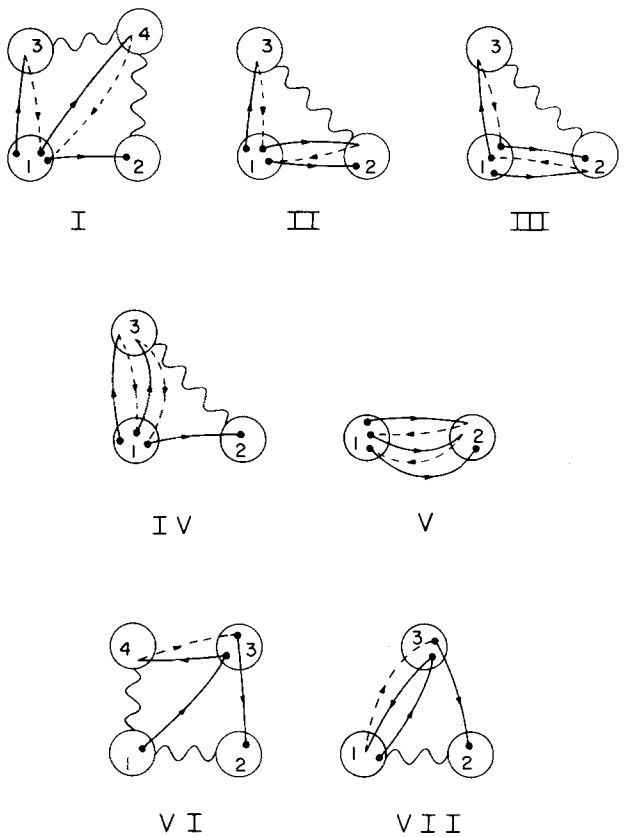

FIG. 8. Diagrams I–V form the complete set of $\Sigma^{(2)}$ diagrams that have V as a reduced diagram. Diagrams VI and VII form the complete set of diagrams that have VII as a reduced diagram.

collapsing of wavy lines in one set of circles is carried out independently of the collapsing of wavy lines in another set. At this point the reader is urged to recall the definition of moveable part in Sec. V. A circle with n moveable parts in a renormalized Σ diagram has an associated polynomial in $-c$ of degree n, denoted $Q_n(c)$. The coefficient of c^m in $Q_n(c)$ is related to the number of ways n moveable parts can be distributed among $m+1$ circles. The combinatorial problem to solve is as follows. We seek the number of ways to put n unlabeled objects (moveable parts) into $m+1$ labeled boxes (circles) such that (i) box 1 may be empty; (ii) each other box has at least one object; (iii) a configuration derived from another by switching the contents of boxes i and j ($i,j \neq 1$) should not be counted as a new configuration. Let P_{mn} be the number of ways of accomplishing the above. Then the coefficient of c^m in $Q_n(c)$ is $(-)^m m! P_{mn}$. The factor $m!$ comes from the singly connected sequence of wavy lines linking the $m+1$ circles. Each wavy line carries a factor -1. P_{mn} is given by

$$P_{mn} = \frac{1}{m!} \sum_{j_1=1} \cdots \sum_{j_m=1} \frac{n!}{j_1! j_2! \cdots j_m! \left(n - \sum_{i=1}^{m} j_i\right)!} \quad \left(\sum_{i=1}^{m} j_i \leqslant n\right) \tag{A1}$$

Equation (A1) can be rewritten in a simpler form. We note that if the $\{j_i\}$ in Eq. (A1) were allowed to take on the value zero, P_{mn} would simply be $(m+1)^n/m!$. We can rewrite Eq. (A1) as a series of sums in which the $\{j_i\}$ start at zero, and then use the multinomial theorem to evaluate each sum in the series. The result is

$$m! P_{mn} = \sum_{i=0}^{m} (-)^i (m+1-i)^n \binom{m}{i}. \tag{A2}$$

$Q_n(c)$ is given by

$$Q_n(c) = \sum_{m=0}^{n} (-c)^m \sum_{i=0}^{m} (-)^i (m+1-i)^n \binom{m}{i}. \tag{A3}$$

The proof that $Q_n(1) = 0$ for $n > 0$ from Eq. (A3) is straightforward. It can also be shown that the $Q_n(c)$ are related to the cumulant polynomials $P_n(c)$ introduced by Yonezawa *et al.*,[17] Leath *et al.*,[18] and Sakun[9] by

$$cQ_n(c) = P_{n+1}(c); \quad n \geqslant 0. \tag{A4}$$

APPENDIX B: SUMMATION OF THE $\Sigma^{(2)}[\mathbf{k}, \hat{G}^s(\epsilon)]$ SERIES

In this Appendix, we evaluate the infinite diagrammatic series $\Sigma^{(2)}[\mathbf{k}, \hat{G}^s(\epsilon)]$, defined in Eq. (V.1), to arrive at Eq. (V.4). It is convenient to divide the $\Sigma^{(2)}$ series into two parts $\Sigma_s^{(2)}[\hat{G}^s(\epsilon)]$ and $\Sigma_d^{(2)}[\mathbf{k}, \hat{G}^s(\epsilon)]$, and sum each part separately. $\Sigma_s^{(2)}$ is the sum of all diagrams in Σ with one field circle and a wavy line between the roots. $\Sigma_s^{(2)}$ is independent of the Fourier vector $\mathbf{k}$. $\Sigma_d^{(2)}$, which is $\mathbf{k}$ dependent, is the sum of all diagrams in Σ with no field circles. We first sum the $\Sigma_s^{(2)}$ series.

The $\Sigma_s^{(2)}$ series is most easily summed by examining a fictitious series $E_s^{(2)}$. The diagrammatic expansion of $E_s^{(2)}$ is identical to that of $\Sigma_s^{(2)}$. The value of an $E_s^{(2)}$ diagram differs from the value of the corresponding $\Sigma_s^{(2)}$ diagram in that instead of associating a polynomial $Q_n(c)$ with each circle, we give a moveable part on root 1 a value m_1, a moveable part on root 2 a value m_2 and a moveable part on the field circle a value m_3. We define a renormalized transfer rate from circle 1 to circle 3 by

$$T_{13} = w_{13} - w_{13}^2 \hat{G}^s(\epsilon) m_3 + w_{13}^3 [\hat{G}^s(\epsilon)]^2 m_3^2 + \cdots = \frac{w_{13}}{1 + w_{13} \hat{G}^s(\epsilon) m_3}. \tag{B1}$$

Similarly, we define T_{32} by

$$T_{32} = \frac{w_{32}}{1 + w_{32} \hat{G}^s(\epsilon) m_3}. \tag{B2}$$

Renormalized return rates R_{31} and R_{32} are given by

$$R_{31} = \frac{-w_{31} \hat{G}^s(\epsilon) m_1}{1 + w_{31} \hat{G}^s(\epsilon) m_3},$$

$$R_{32} = \frac{-w_{32} \hat{G}^s(\epsilon) m_2}{1 + w_{32} \hat{G}^s(\epsilon) m_3}. \tag{B3}$$

Inspection of the diagrams shows that

$$E_s^{(2)} = c\hat{G}^s(\epsilon) \sum_{\mathbf{r}_{12},\mathbf{r}_{13}} (-\delta_{\mathbf{r}_1,\mathbf{r}_2}) \sum_{i=0}^{\infty} T_{13}\, T_{32}(R_{31}+R_{32})^i$$

$$= -c \sum_{\mathbf{r}} \frac{[w(\mathbf{r})]^2 \hat{G}^s(\epsilon)}{[1+w(\mathbf{r})\hat{G}^s(\epsilon)m_3][1+w(\mathbf{r})\hat{G}^s(\epsilon)(m_1+m_2+m_3)]}. \tag{B4}$$

If Eq. (B4) is expanded in powers of $w(\mathbf{r})$, the result is

$$E_s^{(2)} = c \sum_{\mathbf{r}} w(\mathbf{r}) \sum_{k=1}^{\infty} (-z)^k \sum_{i=1}^{k} \binom{k}{i} m_3^{k-i} \sum_{j=0}^{i-1} \binom{i-1}{j} m_1^j\, m_2^{i-j-1}, \tag{B5}$$

where $z \equiv w(\mathbf{r})\hat{G}^s(\epsilon)$, a dimensionless quantity. An $E_s^{(2)}$ diagram with an associated factor $m_1^j m_2^{i-j-1} m_3^{k-i}$ corresponds to a $\Sigma_s^{(2)}$ diagram with an associated factor $Q_j(c)Q_{i-j-1}(c)Q_{k-i}(c)$. We can therefore write

$$\Sigma_s^{(2)}[\hat{G}^s(\epsilon)] = c \sum_{\mathbf{r}} w(\mathbf{r}) \sum_{k=1}^{\infty} (-z)^k \sum_{i=1}^{k} \binom{k}{i} Q_{k-i} \sum_{j=0}^{i-1} \binom{i-1}{j} Q_j Q_{i-1-j}$$

$$\equiv c \sum_{\mathbf{r}} w(\mathbf{r}) \sum_{k=1}^{\infty} (-z)^k A_k(c). \tag{B6}$$

The relationship between the cumulant polynomials of Ref. 9 and the $Q_n(c)$ is given in Appendix A. From this result and Eq. (6) of Ref. 9, we have

$$Q_n(c) = 1/c^2 \frac{d^n}{dx^n}\left(\frac{e^x}{1+e^x}\right)\Big|_{x=\ln(c/1-c)}. \tag{B7}$$

The sum over j in the first line of Eq. (B6) is, therefore,

$$\frac{1}{c^2}\sum_{j=0}^{i-1}\binom{i-1}{j}\left(\frac{d^{i-1-j}}{dx^{i-1-j}}\frac{e^x}{1+e^x}\right)\left(\frac{d^j}{dx^j}\frac{e^x}{1+e^x}\right)\Big|_{x=\ln(c/1-c)} = \frac{1}{c^2}\frac{d^{i-1}}{dx^{i-1}}\left(\frac{e^x}{1+e^x}\right)^2\Big|_{x=\ln(c/1-c)}, \tag{B8}$$

where Leibnitz' rule has been applied. The quantity $A_k(c)$ defined in Eq. (B6) is given by

$$A_k(c) = 1/c^3 \sum_{i=1}^{k}\binom{k}{i}\left(\frac{d^{k-i}}{dx^{k-i}}\frac{e^x}{1+e^x}\right)\left(\frac{d^{i-1}}{dx^{i-1}}\left(\frac{e^x}{1+e^x}\right)^2\right)\Big|_{x=\ln(c/1-c)}. \tag{B9}$$

Application of Leibnitz' rule to this expression gives

$$A_k(c) = 1/c^3 \frac{d^k}{dx^k}\left[\frac{e^x}{1+e^x}\right]\left[\ln(1+e^x) - \frac{e^x}{1+e^x} + c + \ln(1-c)\right]\Big|_{x=\ln(c/1-c)}. \tag{B10}$$

The sum over k in Eq. (B6) can be evaluated using the generating function technique of Yonezawa and Matsubara.[14] We seek a function $g(y,c)$ such that

$$g(y,c) = \sum_{k=1}^{\infty} A_k(c)\, y^k/k!, \tag{B11}$$

which implies

$$A_k(c) = \frac{d^k}{dy^k} g(y,c)\Big|_{y=0}. \tag{B12}$$

Equation (B10) can be rewritten as

$$A_k(c) = \frac{d^k}{dy^k}\left(\frac{1}{c^3}\right)\left[\frac{e^{x+y}}{1+e^{x+y}}\right]\left[\ln(1+e^{x+y}) - \frac{e^{x+y}}{1+e^{x+y}} + c + \ln(1-c)\right]\Big|_{\substack{y=0\\ x=\ln(c/1-c)}}$$

$$= \frac{d^k}{dy^k}\left(\frac{1}{c}\right)\left[\frac{e^y}{1-c+ce^y}\right]\left[\frac{1}{c}\ln(1-c+ce^y) + \frac{(1-c)(1-e^y)}{1-c+ce^y}\right]\Big|_{y=0}. \tag{B13}$$

From Eqs. (B12) and (B13), we can make the identification

$$g(y,c) = \frac{1}{c}\left[\frac{e^y}{1-c+ce^y}\right]\left[\frac{1}{c}\ln(1-c+ce^y) + \frac{(1-c)(1-e^y)}{1-c+ce^y}\right]\Big|_{y=0} + \text{const}. \tag{B14}$$

The constant is determined to be zero from the initial condition $g(0,c)=0$. Substituting $y\alpha$ for y in Eq. (B11), multiplying through by $e^{-\alpha}$ and integrating both sides from $\alpha = 0$ to $\alpha = \infty$ gives

$$\int_0^{\infty} d\alpha\, e^{-\alpha} g(y\alpha,c) = \sum_{k=1}^{\infty} A_k(c)\, y^k. \tag{B15}$$

The right-hand side of Eq. (B15) is the sum we seek in Eq. (B6). Substituting Eqs. (B14) and (B15) into Eq. (B6) yields

$$\sum_s^{(2)}[\hat{G}^s(\epsilon)] = \sum_{\mathbf{r}} w(\mathbf{r}) \int_0^{\infty} d\alpha\, e^{-\alpha}\left(\frac{e^{-z\alpha}}{1-c+ce^{-z\alpha}}\right)\left[\frac{1}{c}\ln(1-c+ce^{-z\alpha}) + \frac{(1-c)(1-e^{-z\alpha})}{1-c+ce^{-z\alpha}}\right], \tag{B16}$$

where $z \equiv w(\mathbf{r})\hat{G}^s(\epsilon)$.

The procedure just used to sum the $\Sigma_s^{(2)}$ series can be applied to the summation of $\Sigma_d^{(2)}$. Diagrams in this series have 2 root circles and no field circles. We first treat a fictitious series $E_d^{(2)}$, that bears the same relation to $\Sigma_d^{(2)}$ as $E_s^{(2)}$ does to $\Sigma_s^{(2)}$. The value of an $E_d^{(2)}$ diagram with n moveable parts on circle 1 and p moveable parts on circle 2 has a factor $m_1^n m_2^p$. Renormalized transfer and return rates are defined by

$$T_{12} = \frac{w_{12}}{1 + w_{12}\hat{G}^s(\epsilon)m_1},$$
$$R_{12} = \frac{-w_{12}\hat{G}^s(\epsilon)m_2}{1 + w_{12}\hat{G}^s(\epsilon)m_1}. \tag{B17}$$

Inspection of the diagrammatic series $E_d^{(2)}$ shows that it can be expressed as

$$E_d^{(2)} = \sum_{\mathbf{r}_{12}} e^{i\mathbf{k}\cdot\mathbf{r}_{12}} T_{12} \sum_{n=0}^{\infty} R_{12}^n . \tag{B18}$$

Substitution of expressions (B17) into Eq. (B18) gives

$$E_d^{(2)} = \sum_{\mathbf{r}} e^{i\mathbf{k}\cdot\mathbf{r}} \frac{w(\mathbf{r})}{1 + w(\mathbf{r})\hat{G}^s(\epsilon)(m_1 + m_2)}. \tag{B19}$$

Expanding the summand in powers of $w(\mathbf{r})$ gives

$$E_d^{(2)} = \sum_{\mathbf{r}} e^{i\mathbf{k}\cdot\mathbf{r}} w(\mathbf{r}) \sum_{n=0}^{\infty} (-z)^n \sum_{i=0}^{n} \binom{n}{i} m_1^i m_2^{n-i}, \tag{B20}$$

where $z = w(\mathbf{r})\hat{G}^s(\epsilon)$.

An $E_d^{(2)}$ diagram whose value contains a factor $m_1^i m_2^{n-i}$ corresponds to a $\Sigma_d^{(2)}$ diagram whose value contains a factor $Q_i(c)Q_{n-i}(c)$. The series $\Sigma_d^{(2)}$ therefore has the value

$$\sum_d^{(2)} [\mathbf{k}, \hat{G}^s(\epsilon)]$$
$$= \sum_{\mathbf{r}} e^{i\mathbf{k}\cdot\mathbf{r}} w(\mathbf{r}) \sum_{n=0}^{\infty} (-z)^n \sum_{i=0}^{n} \binom{n}{i} Q_i(c)Q_{n-i}(c)$$
$$\equiv \sum_{\mathbf{r}} e^{i\mathbf{k}\cdot\mathbf{r}} w(\mathbf{r}) \sum_{n=0}^{\infty} (-z)^n S_n(c). \tag{B21}$$

Applying Eq. (B7) and Leibnitz' rule yields

$$S_n(c) = 1/c^2 \frac{d^n}{dx^n} \left(\frac{e^x}{1 + e^x} \right)^2 \Bigg|_{x = \ln(c/1-c)}. \tag{B22}$$

The sum over n in Eq. (B21) can be carried out using the generating function technique described above. We seek a function $h(c,y)$ such that

$$h(c,y) = \sum_{n=0}^{\infty} S_n(c)\, y^n/n!, \tag{B23}$$

which implies

$$S_n(c) = \frac{d^n}{dy^n} h(c,y) \Big|_{y=0}. \tag{B24}$$

Equation (B22) can be rewritten as

$$S_n(c) = \frac{d^n}{dy^n} \frac{1}{c^2} \left[\frac{e^{x+y}}{1 + e^{x+y}} \right]^2 \Bigg|_{\substack{y=0 \\ x=\ln(c/1-c)}}$$
$$= \frac{d^n}{dy^n} \left[\frac{e^y}{1 - c + ce^y} \right]^2 \Bigg|_{y=0}. \tag{B25}$$

Comparison of Eqs. (B24) and (B25) yields

$$h(c,y) = \left[\frac{e^y}{1 - c + ce^y} \right]^2. \tag{B26}$$

Replacing y by $y\alpha$ in Eq. (B23), multiplying through by $e^{-\alpha}$ and integrating both sides from $\alpha = 0$ to $\alpha = \infty$ gives

$$\int_0^{\infty} d\alpha\, e^{-\alpha} h(c, y\alpha) = \sum_{n=0}^{\infty} S_n(c)\, y^n. \tag{B27}$$

Substituting Eqs. (B26) and (B27) into Eq. (B21) gives

$$\sum_d^{(2)} [\mathbf{k}, \hat{G}^s(\epsilon)]$$
$$= \sum_{\mathbf{r}} e^{i\mathbf{k}\cdot\mathbf{r}} w(\mathbf{r}) \int_0^{\infty} d\alpha\, e^{-\alpha} \left(\frac{e^{-z\alpha}}{1 - c + ce^{-z\alpha}} \right)^2, \tag{B28}$$

where $z = w(\mathbf{r})\hat{G}^s(\epsilon)$.

The integrals in Eqs. (B28) and (B16) must be done numerically. Substituting Eqs. (B16) and (B28) into the relation

$$\sum^{(2)} [\mathbf{k}, \hat{G}^s(\epsilon)] = \sum_d^{(2)} [\mathbf{k}, \hat{G}^s(\epsilon)] + \sum_s^{(2)} [\hat{G}^s(\epsilon)]$$

results in the expression presented in Eq. (V.4).

APPENDIX C: A TOPOLOGICAL THEOREM

In this Appendix, we prove a theorem that is used in the renormalization of the $\Sigma^{(2)}[\mathbf{k}, \hat{G}^s(\epsilon)]$ series described in Appendix A. The theorem is most easily stated in terms of a new type of diagram composed only of circles and wavy lines. Such a diagram is constructed by linking n distinguishable circles with wavy lines in such a way that each pair of circles is connected in the sense of Ref. 13, and that no pair of circles is directly connected by more than one wavy line. A direct connection between two circles is a wavy line whose ends are attached to the circles. We denote the sum of all such diagrams Λ_n. Each diagram in Λ_n has a value $(-1)^p$, where p is the number of wavy lines in the diagram. Since each diagram has value 1 or -1, there will be considerable cancellation among the diagrams in Λ_n.

Consider an arbitrary division of the circles into two groups. j circles are designated branch circles and $n-j$ circles are designated trunk circles, where $j \geq 1$. Since the circles are distinguishable, we can label the trunk circles 1 through $n-j$ and the branch circles $n-j+1$ through n. A subset of the diagrams in Λ_n have the following features. The trunk circles are linked by a singly connected path of wavy lines constructed by drawing a wavy line from each of circles 1 through $n-j-1$ to the circle with the next highest valued numerical label. The branch circles are divided into sets. Each set is linked by a singly connected path of wavy lines constructed by drawing a wavy line from each circle (except for the circle with the highest valued numerical label) to the circle whose numerical label has the next highest value. The branch circle with the lowest valued numerical label in each set is also connected to one of the trunk circles. Each trunk circle can have at most one such connection. Let the sum of this subset of Λ_n diagrams be denoted λ_n. Our theorem states that if we evaluate each λ_n diagram with the following rules, then the value of the original Λ_n series equals the value of this new λ_n series. Each wavy line contributes a factor of -1. The set of $n-j$ trunk circles contributes a factor

$(n-j-1)!$. Each set of s branch circles contributes a factor $s!$.

We now prove this result. We have defined the notions of "connection" and "direct connection". We now define an indirect connection as any connection that is not direct. Consider diagrams in Λ_n in which circle 1 is indirectly connected to another trunk circle by a sequence of wavy lines and circles that contains one or more branch circles. If there is more than one such connection consider the connection linking circle 1 to the trunk circle whose numerical label has the lowest value. Let this lowest number be k. Either there exists a direct connection between circles 1 and k or there does not. Consider a diagram in which this connection exists. There exists a second diagram in Λ_n that differs from the first only in that this direct connection is absent. The value of the sum of this pair of diagrams is zero. Therefore, in summing Λ_n, we need not consider any diagram in which circle 1 is connected to any of the other trunk circles by a sequence of wavy lines and circles that includes one or more branch circles. Similarly, we can eliminate all diagrams in which circle 2 is connected to any of the trunk circles labeled 3 through $n-j$ by a sequence of lines and circles that includes one or more branch circles. This procedure can be applied to the circles labeled 3 through $n-j-1$. The only diagrams remaining in Λ_n are ones in which the trunk circles are completely connected and the branch circles are divided into sets with the following characteristics. Circles in one set are not connected to circles in another. At least one circle in each set is connected directly to a trunk circle. Other circles in the set may be connected directly to that same trunk circle but may not be directly connected to any other trunk circle. Each set of branch circles and the single trunk circle to which circles in the set may be directly connected forms a completely connected set of circles. A set of circles is completely connected if each pair of circles in the set is connected.

Consider a completely connected group of m circles in such a diagram. Let this group be either the entire group of trunk circles or a set of branch circles and the trunk circle to which it is directly connected. In the former case, let us refer to trunk circle 1 as circle q. In the latter case let circle q be the single trunk circle to which the branch circles may be directly connected. Let circle q be directly connected to the set of circles $(i,j,...z)$, where i is the label with the lowest numerical value and z is the label with the highest numerical value. Let circles i and z be directly connected. For each diagram containing this structure, there exists another diagram that differs from it only in that the direct connection from i to z is absent. The value of the sum of this pair is zero. Therefore we need only retain diagrams in which circle q has a single wavy line attached to it. Let the circle to which it is attached be labeled k. The same arguments allow us to retain only diagrams in which circle k is connected to one other circle. By repeating this argument we reduce the set of diagrams in Λ_n to those in which the m circles are linked by a singly connected path of wavy lines that starts on circle q. There are $(m-1)!$ such paths. We can represent these $(m-1)!$ possibilities with a single path constructed by drawing wavy lines from each circle (except for the circle whose label has the highest numerical value) to the circle whose label has the next highest numerical value. When the diagram is evaluated this path contributes a factor $(m-1)!$.

Consider the remaining Λ_n diagrams. The procedure just described can be applied independently to the trunk circles and to each set of branch circles. The resulting diagrammatic series is exactly λ_n, in which each diagram is evaluated by the rules given in the statement of the theorem.

[1] G. Pfister and H. Scher, Phys. Rev. B **15**, 2062 (1977).

[2] G. P. Pfister, S. Grammatica, and J. Mort, Phys. Rev. Lett. **37**, 1360 (1976); H. Scher and C. Wu, Proc. Natl. Acad. Sci. U.S.A. **78**, 22 (1981).

[3] R. Kopelman, in *Topics in Applied Physics*, edited by W. M. Yen and P. M. Seltzer (Springer, Berlin, 1981), Vol. 49, p. 241; S. D. Colson, S. M. George, T. Keyes, and V. Vaida, J. Chem. Phys. **67**, 4941 (1977).

[4] C. R. Gochanour and M. D. Fayer, J. Phys. Chem. **85**, 1989 (1981); R. J. D. Miller, M. Pierre, and M. D. Fayer, J. Chem. Phys. **78**, 5138 (1983).

[5] K. Sauer, Annu. Rev. Phys. Chem. **30**, 155 (1979).

[6] W. Klöpffer, Ann. N. Y. Acad. Sci. **366**, 373 (1981); M. D. Ediger and M. D. Fayer, Macromolecules **16**, 1839 (1983); G. H. Fredrickson, H. C. Andersen, and C. Frank, J. Chem. Phys. **79**, 3572 (1983).

[7] (a) S. W. Haan and R. Zwanzig, J. Chem. Phys. **68**, 1879 (1978); (b) J. Klafter and R. Silbey, *ibid.* **72**, 843 (1980); (c) K. Godzik and J. Jortner, *ibid.* **72**, 4471 (1980); (d) D. L. Huber, Phys. Rev. B **20**, 2307, 5333 (1979).

[8] C. R. Gochanour, H. C. Andersen, and M. D. Fayer, J. Chem. Phys. **70**, 4254 (1979).

[9] V. Sakun, Sov. Phys. Solid State **14**, 1906 (1973).

[10] (a) T. Odagaki and M. Lax, Phys. Rev. B **24**, 5284 (1981); M. Lax and T. Odagaki, in *Lecture Notes in Physics*, edited by R. Burridge, S. Childress, and G. Papanicolaou (Springer, Berlin, 1982), Vol. 154, p. 148; (b) G. Korzeniewski, R. Friesner, and R. Silbey, J. Stat. Phys. **31**, 451 (1983).

[11] (a) Th. Förster, Ann. Phys. (Leipzig) **2**, 55 (1948); (b) D. L. Dexter, J. Chem. Phys. **21**, 836 (1953); (c) A. Miller and E. Abrahams, Phys. Rev. **120**, 745 (1960).

[12] R. F. Loring, Hans C. Andersen, and M. D. Fayer, Phys. Rev. Lett. **50**, 1324 (1983). An error was made in arriving at Eq. (4) of this work, which should be replaced by Eq. V.4 of the present work. The specification of the diagrammatic series in (Ref. 12) should be replaced by the discussion in Secs. IV and V of this paper. The effect of this error on the numerical results presented in Fig. 1 of Ref. 12 is negligible within the precision of the figure.

[13] The notion of connectivity used here is similar to that traditionally used in graphical analysis of physical problems. A circle should be regarded as connected to any wavy line attached to it and connected to any arrow that lead to or away from the interior of the circle. If a circle contains the starting and ending points of several arrows, these starting and ending points should be regarded as connected. Two objects connected to the same third object should be regarded as connected to one another.

[14] In the present problem, loops can also be defined in the following way. A loop is a subset of the arrows, circles, and wavy lines of a diagram, with the following properties. The arrows in a loop are a continuous path of arrows that begins and ends on vertices in the same circle. The circles in a loop are the circles that the path visits, with the exception of the circle on which it starts and ends. The wavy lines in the loop are all wavy lines between circles in the loop and all wavy lines between circles in the loop and the circle on which the loop starts and ends. The circles in the loop are visited by no arrows other than the arrows in the loop. The circles in the loop may be connected by wavy lines only to other circles in the loop and to the circle on which the loop starts and ends. This definition of loop is a generalization of that of GAF to the present case of diagrams that may have wavy lines connecting the circles.

[15] A node can also be defined in the following way. The path of arrows from one root to the other passes through each vertex once. Each vertex can be used to break the total path into two parts. The first part is between the start of the path at root 1 and the vertex. The second part is between the vertex and the end of the path at root 2. The vertex is a node if the following two conditions are satisfied. First, the only circle visited on both parts of the path is the circle containing the vertex. Second, there is no wavy line in the diagram with the property that one end is attached to a circle visited before the circle containing the vertex and the other end is attached to a

circle visited after the circle containing the vertex.
[16]D. A. McQuarrie, *Statistical Mechanics* (Harper and Row, New York, 1976), p. 580.
[17]F. Yonezawa and T. Matsubara, Prog. Theor. Phys. **35**, 357 (1966).
[18]P. L. Leath and B. Goodman, Phys. Rev. **148**, 968 (1966).
[19]Y. Wong, Ph.D. thesis, University of Rochester, Rochester, New York, 1979.
[20]For any $n > 2$, the n body approximation includes the diagrams in the two body approximation and hence contains the exactly correct answer at $c = 1$. The important question is whether the remaining diagrams can be shown not to contribute at $c = 1$. Demonstration of this requires carrying out the same sort of renormalization as is carried out in Appendix A for the diagrams in the two body approximation and showing that every $\mathbf{k}$ dependent diagram has at least one factor of Q_j for $j > 0$. We suspect that this renormalization can be carried out, but it is rather complicated and we have not yet been able to do it.
[21]M. A. Barber and B. W. Ninham, *Random and Restricted Walks* (Gordon and Breach, New York, 1970).
[22]H. Stehfest, Commun. Assoc. Comp. Mach. **13**, 47, 624 (1970).
[23]R. Loring (unpublished results).
[24](a) S. Kirkpatrick, Phys. Rev. Lett. **36**, 69 (1976); (b) M. F. Sykes, D. S. Gaunt, and M. Glen, J. Phys. A **9**, 1705 (1976).
[25]Korzeniewsky, Friesner, and Silbey [Ref. 10(b)] have shown that for a nearest neighbor transfer rate, the two site EMA yields identical results for the site disorder problem they treat and for the bond disorder problem treated by Odagaki and Lax [Ref. 10(a)].